DOI: 10.1002/smll.200701043

Functionalized-Quantum-Dot–Liposome Hybrids as Multimodal Nanoparticles for Cancer**

*Wafa' T. Al-Jamal, Khuloud T. Al-Jamal, Paul H. Bomans, Peter M. Frederik, and Kostas Kostarelos**

***F**unctionalized-quantum-dot–liposome (f-QD-L) hybrid nanoparticles are engineered by encapsulating poly(ethylene glycol)-coated QD in the internal aqueous phase of different lipid bilayer vesicles. f-QD-L maintain the QD fluorescence characteristics as confirmed by fluorescence spectroscopy, agarose gel electrophoresis, and confocal laser scanning microscopy. Cationic f-QD-L hybrids lead to dramatic improvements in cellular binding and internalization in tumor-cell monolayer cultures. Deeper penetration into three-dimensional multicellular spheroids is obtained for f-QD-L by modifying the lipid bilayer characteristics of the hybrid system. f-QD-L are injected intratumorally into solid tumor models leading to extensive fluorescent staining of tumor cells compared to injections of the f-QD alone. f-QD-L hybrid nanoparticles constitute a versatile tool for very efficient labeling of cells ex vivo and in vivo, particularly when long-term imaging and tracking of cells is sought. Moreover, f-QD-L offer many opportunities for the development of combinatory therapeutic and imaging (theranostic) modalities by incorporating both drug molecules and QD within the different compartments of a single vesicle.*

Keywords:
- liposomes
- quantum dots
- spheroid penetration
- tumor imaging
- theranostics

1. Introduction

Fluorescent cell labeling allows monitoring of cell migration and behavior (e.g., differentiation) in vitro and in vivo.[1] Many approaches have been developed to label cells by microinjection with organic fluorophores or by transfecting cells with reported genes that code for luciferase or fluorescent proteins such as GFP.[2] Quantum dots (QD) are considered promising fluorescent nanoprobes due to their fluorescence intensity, narrow emission, tunable spectra, and higher photostability compared to conventional organic fluorophores.[3] QD have been increasingly explored for various biomedical applications,[4,5] including cell labeling and tracking.[6–10] Much effort has been made to improve the cellular uptake of QD in vitro and in vivo by functionalization of the QD surface using biological molecules by noncovalent, electrostatic adsorption onto the QD surface[11] and by covalent attachment.[12]

The need for effective approaches to label cells has emerged since minimum cell labeling was observed with nonfunctionalized QD.[13,14] Jaiswal and co-workers reported nonspecific labeling of HeLa cells incubated for 2–3 h with 400–600 nM dihydrolipoic acid (DHLA)-coated QD.[11] However, better cell labeling was obtained at lower QD doses via electroporation,[13,15] microinjection[9,13] or by using surface-functionalized QD.[16–23] A wide variety of QD surface functionalizations have been reported by conjugation of different ligands such as proteins,[24] antibodies,[20,21,25]

[*] Prof. K. Kostarelos, W. T. Al-Jamal, Dr. K. T. Al-Jamal
Nanomedicine Laboratory, Centre for Drug Delivery Research
The School of Pharmacy
University of London
29–39 Brunswick Square, London WC1N 1AX (UK)
E-mail: kostas.kostarelos@pharmacy.ac.uk
P. H. Bomans, Dr. P. M. Frederik
Electron Microscopy Facility, Department of Pathology
University of Maastricht Medical School
Maastricht (The Netherlands)

Supporting Information is available on the WWW under http://www.small-journal.com

NANO MICRO small

peptides,[6,17,19] endosome-disruptive polymers,[23] aptamers,[16] and cell-penetrating peptides.[18,22,26–29]

In an alternative approach, preformed liposomes of cationic surface character have been electrostatically complexed with functionalized QD (*f*-QD) to enhance the cellular uptake of *f*-QD for cell labeling and tracking purposes.[10,13] These studies attempted simple mixing protocols between commercially available liposome-based transfection agents (such as Lipofectamine 2000) and *f*-QD in order to translocate enough QD particles intracellularly.

Towards applications that aim at in vivo tumor cell labeling and tracking, a critically important problem is the limited retention of QD in the tumor volume even after intratumoral administrations[30] and their translocation and drainage to the lymphatic system. Such strategies currently require high does of injected QD to maintain adequate fluorescence contrast in the tumor[30] increasing toxicological burden from cadmium accumulation. A few studies have also achieved QD targeting of tumor xenografts by intravenous administration, by either active or passive targeting strategies;[6,8,17,21,25] however, in all previous studies very high doses of QD had to be injected to achieve efficient tumor cell labeling.

In the present work we report the engineering of a new type of nanoparticle by encapsulating COOH–PEG–QD (PEG: poly(ethylene glycol)) into small unilamellar lipid vesicles (SUV) of various lipid compositions. Such *f*-QD–liposome hybrid nanoparticles (*f*-QD-L) have been developed with the specific aims of enhancing internalization into tumor cells, achieving a high degree of penetration through the tumor interstitium, and increasing retention within the tumor mass in vivo, which will allow for efficient labeling of cancer cells and dramatically reduce the dose of QD needed. Moreover, such hybrid systems are designed to take advantage of the physicochemical and pharmacodynamic versatility offered by the liposome structure[31] combined with the wide range of photochemical characteristics of the different available types of *f*-QD.

2. Results

2.1. Preparation and Characterization of *f*-QD-L

f-QD-L hybrids were prepared by following well-established liposome preparation protocols and incorporation of the nanocrystals at various stages. Film hydration followed by bath sonication was chosen as the preferred method of *f*-QD-L preparation. Minimal changes in the average particle size and fluorescence intensity of COOH–PEG–QD were observed from such processing as confirmed by dynamic light scattering (DLS), fluorescence spectrophotometry, and agarose gel electrophoresis (see Supporting Information, Figure S1).

DLS was used to determine the average size and surface charge of *f*-QD and the *f*-QD-L hybrids using zwitterionic [DOPC] and cationic [DOPC:DC-Chol (10:1)] lipids (Figure 1). The aqueous dispersion of *f*-QD alone exhibited an average diameter of 40 nm and a weak negative surface charge (−7.63 mV; Figure 1A). Cryo-transmission electron microscopy (cryo-TEM) revealed individualized 15–20-nm COOH-PEG-QD particles, indicating that each *f*-QD consisted of 2–3 nanocrystals coated by the lipopolymer (Figure 1B). Such discrepancies between the hydrodynamic diameter determined by DLS and the average *f*-QD size determined by cryo-TEM have also been previously reported by others[32,33] and are due to the measured hydrodynamic diameter in the case of DLS.[34] Incorporation of the hydrophilic *f*-QD into different vesicles resulted in *f*-QD-L hybrid nanoparticles 80–100 nm in average diameter, as determined by both DLS and cryo-TEM (Figure 1C and D, respectively) with a wide size distribution, as expected from such preparation protocols. The surface charge characteristics of the *f*-QD-L hybrids were in accordance with the characteristics of the lipid molecules used to form the bilayers (Figure 1C and Table 1).

Cryo-TEM of the *f*-QD-L hybrids (Figure 1D) indicated clearly that vesicular structures were formed and that several *f*-QD were incorporated into each vesicle. It was also consistently observed that the *f*-QD were interacting with the lipid bilayer (see black arrows in Figure 1D) rather than being simply encapsulated into the vesicle inner aqueous compartment, suggesting some degree of lipid mixing between the bilayer lipids and the lipopolymer on the *f*-QD surface. Interestingly, the incorporation of the *f*-QD into liposomes led to vesicular structures that were fluorescent (Figure 2). The fluorescence intensity of *f*-QD-L hybrids was lower than that of *f*-QD alone in water (for the same total concentration of QD) and the peak shifted slightly towards the red emission wavelengths. These changes in the *f*-QD optical properties upon incorporation with the liposomes are thought to be due to the ensuing interaction between the *f*-QD and the lipid bilayer (as evidenced by cryo-TEM).

2.2. *f*-QD Loading Efficiency in the Hybrid Nanoparticles

The effect of different molar ratios between lipids and *f*-QD on *f*-QD-L formation was investigated using agarose gel electrophoresis. Migration in the gel matrix is dependent on the size and the surface charge of the particle of interest. *f*-QD alone showed distinctive fluorescent band migration in the gel toward the positive electrode (Figure 3A, lane I). The formation of *f*-QD-L hybrid nanoparticles was evidenced (Figure 3A) by the lack of *f*-QD migration in the agarose gel. The fluorescent *f*-QD-L were immobilized into the well of the gel, while free *f*-QD migrated toward the positive electrode. In a control experiment, simple mixing at the same molar ratios between preformed DOPC SUV with *f*-QD did not produce hybrid nanoparticles, as evidenced by the presence of the free *f*-QD band across the gel (Figure 3B).

Moreover, this technique was used to reveal the *f*-QD:lipid molar ratio to obtain maximum loading of the *f*-QD within the *f*-QD-L system. Lipid concentrations of 0.4 mM and 4 mM resulted in the presence of free *f*-QD (Figure 3A, lanes II and III, respectively), while lipid concentrations of 8 mM and 20 mM led to complete lack of *f*-QD migration (Figure 3A, lanes IV and V, respectively). Similar retardation of *f*-QD in agarose gels has been previously reported by others[15,35] following conjugation or coating with uncharged polymers or proteins. A recent study by Srinivasan et al. also reported that simple mixing of PEGylated QD with DNA did not prevent

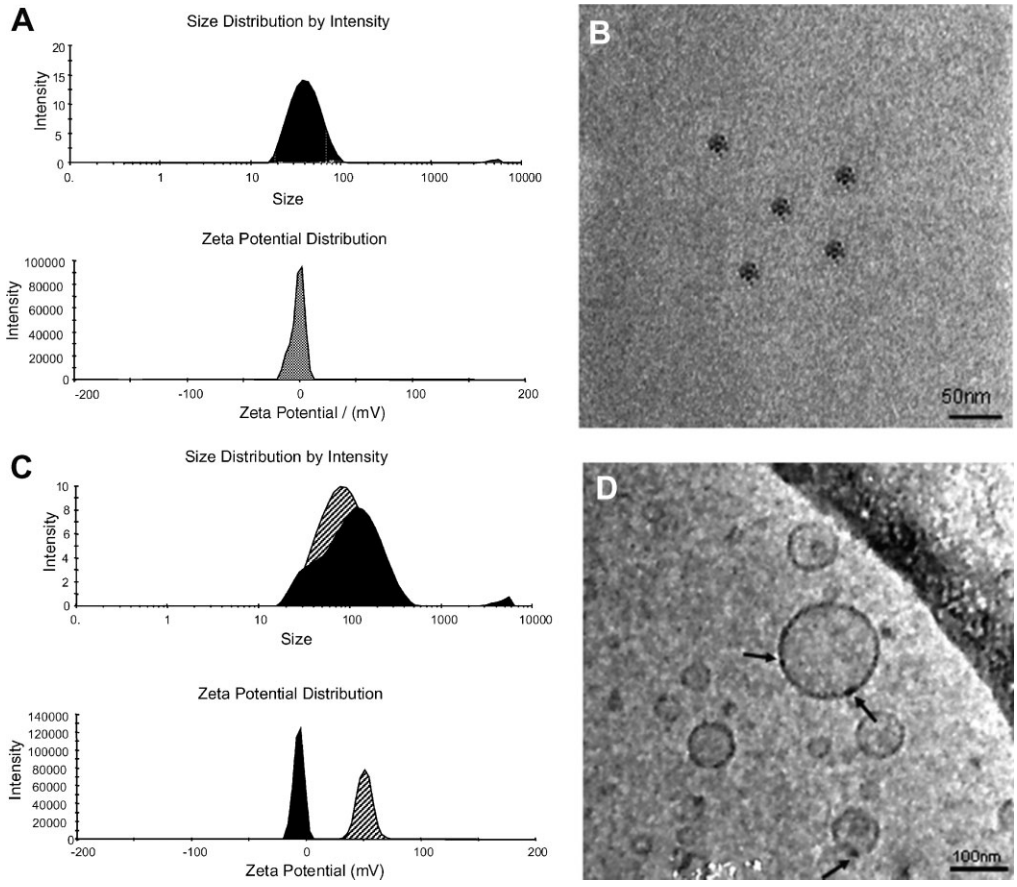

Figure 1. *f*-QD and *f*-QD-L nanoparticle characteristics. Average diameter found by DLS and ξ potential of A) *f*-QD and C) *f*-QD-L (DOPC, black filled curve; DOPC-DC-Chol (10:1), striped curve). (B) and (D) show cryo-TEM images of *f*-QD and *f*-QD-L (DOPC), respectively.

migration of the *f*-QD in agarose gels; however, once the *f*-QD were covalently attached to DNA, immobilization was observed due to the high molecular weight of the QD-DNA conjugate.[5] In the present study, we believe that lack of migration is due to the larger average size of the resulting *f*-QD-L hybrids, since neither zwitterionic nor cationic fluorescently (DiI)-labeled SUV could migrate in the agarose gel under these conditions (data not shown).

2.3. Tumor-Cell Internalization of *f*-QD-L Hybrid Nanoparticles

f-QD and *f*-QD-L were allowed to interact with human-lung epithelial carcinoma A549 cells, incubated with increasing final concentrations of 1.8, 3.6 and 7.2 mM of total lipid loaded with 40, 80 and 145 nM *f*-QD, respectively (Figure 4). For this study, the cationic analogue of cholesterol was incorporated in the *f*-QD-L bilayers to enhance the interaction with the plasma membrane. *f*-QD alone at this concentration range did not show any intracellular signal, indicating that no uptake by A549 cells took place even after 3 h of incubation (Figure 4A–C).

This was attributed to the steric hindrance by the PEG coat that reduced the nonspecific *f*-QD cell binding and the low concentration of *f*-QD used. In contrast, the cationic *f*-QD-L (DOPC:DC-Chol) hybrids were internalized by A549 cells very efficiently. This uptake was shown to be dose- and time-dependent (Figure 4D–F). Within 1 h, *f*-QD-L were bound to the cell membrane (see Supporting Information, Figure S2). After 3 h incubation, *f*-QD-L were capable of intracellular

Table 1. Size and surface-charge characteristics of different *f*-QD-L hybrids used in this study. The average diameter, polydispersity index, and surface charge of *f*-QD-L were obtained using the Nanosizer ZS.

QD-L Nanoparticle type	Average diameter [nm ± S.D.][a]	Polydispersity index ± S.D.[a]	Surface charge [mV ± S.D.][a]
DOPC	87.4 ± 0.91	0.349 ± 0.036	−7.86 ± 0.721
DOPC:Chol (2:1)	92.3 ± 1.28	0.270 ± 0.002	−10.3 ± 1.99
DOPC:DOPE:Chol (2:1:1.5)	87.2 ± 0.298	0.298 ± 0.001	−16.7 ± 0.319
DOPC:DC-Chol (10:1)	81.6 ± 0.579	0.287 ± 0.002	+56.1 ± 1.48
DOPC:DOPE:Chol:DC-Chol (2:1:1.5:0.3)	87.6 ± 0.882	0.276 ± 0.004	+51.9 ± 1.28

[a] Mean ± standard deviation; $n = 3$.

NANO MICRO small

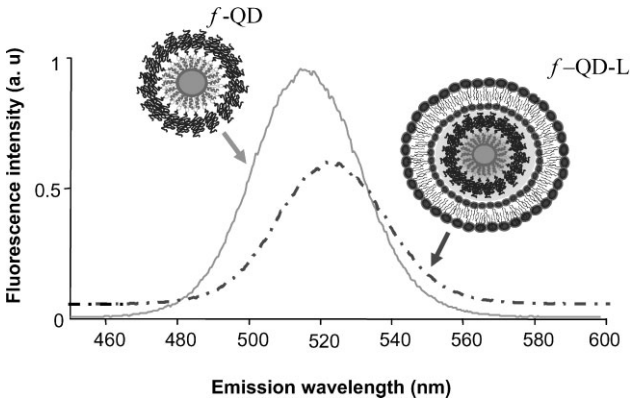

Figure 2. The fluorescence emission spectra of COOH-PEG-QD (continuous line) and *f*-QD-L (DOPC) nanoparticles (dashed line) and the equivalent schematic depiction of *f*-QD and *f*-QD–L hybrids. Note that the structures depicted schematically are not drawn to scale.

trafficking presumably via endosomal uptake (as has been described in numerous studies for positively charged liposomes) and could be imaged throughout the cell volume and close to the nucleus (Figure 4F). Contrary to that, the *f*-QD-L in the absence of a positive surface charge (DOPC alone) did not show high levels of cellular uptake even after 3 h of incubation with the same cells (data not shown). Similar observations were reported by others when QD coated with cationic surfactants, such as di-dodecyl (C12) or di-hexadecyl (C16) di-methylammonium bromide, showed high cellular uptake compared to lecithin coated QD.[26] Our studies herein suggest that the positive charge is a key parameter responsible for increased cellular uptake of the *f*-QD-L hybrid system.

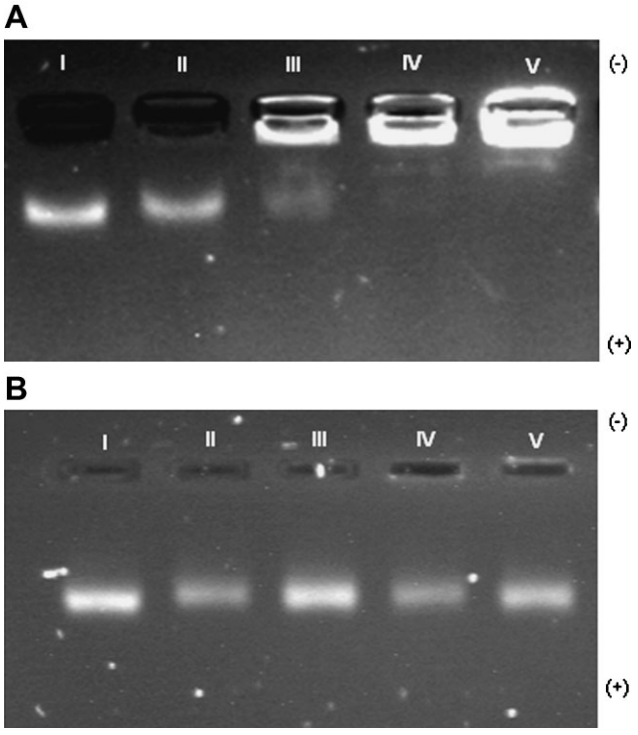

Figure 3. Encapsulation of *f*-QD (COOH-PEG-QD) into lipid vesicles at different molar ratios. Migration profile in 1% agarose and 0.5× TBE buffer of A) *f*-QD-L and B) *f*-QD and SUV mixed controls at 0 mM DOPC (lane 1), 0.4 mM (lane II), 4 mM (lane III), 8 mM (lane IV), and 20 mM (lane V). The free *f*-QD band in the gel disappears at 8 mM DOPC, indicating complete *f*-QD incorporation into the *f*-QD-L vesicles.

2.4. Three-Dimensional Multicellular Tumor Spheroid Penetration of *f*-QD-L Hybrid Nanoparticles

In order to design *f*-QD-L hybrid for efficient tumor uptake, localization, and labeling, apart from efficient tumor-cell internalization the capability of *f*-QD-L to penetrate and diffuse into tumor mass has to be modulated. Despite efforts for the development of QD for tumor-cell targeting and tagging, no study has previously reported the interaction between nonfunctionalized or functionalized QD and the solid tumor mass. Multicellular tumor spheroids (MCS) are particularly useful models that mimic the avascular interstitial tumor space[36] that nanoparticles, such as the *f*-QD-L developed here, need to transport through in vivo. To explore this, we used three-dimensional (3D) MCS cultures from melanoma cells (B16F10). *f*-QD were incubated with the tumor MCS for 4 h at 37 °C, followed by thorough washing to remove any unbound nanoparticle prior to confocal laser scanning microscopy (CLSM) imaging. Similar to the observed interactions between *f*-QD and cells in monolayer cultures (Figure 4), steric hindrance from the PEG coat prevented *f*-QD interaction and penetration with the tumor cells cultured as MCS (Figure 5B). Despite the small size of the *f*-QD (15–30 nm), the lack of any binding, association, or diffusion throughout the MCS volume is in full agreement with previous studies that reported complete lack of interaction between PEGylated nanoscale-sized (below 100 nm) empty liposomes and MCS.[37]

In order to obtain optimum binding and penetration into the MCS mass, we engineered the *f*-QD-L characteristics according to previous findings for liposomes alone,[37] and more relevant to the clinical setting. The *f*-QD-L that were allowed to interact with the tumor spheroids consisted of cholesterol (Chol) to enhance the liposome stability in vivo,[38] and the fusogenic lipid DOPE. After 4 h of incubation, cationic *f*-QD-L consisting of DOPC:DOPE:Chol:DC-Chol (2:1:1.5:0.3) and a final concentration of 145 nM QD, with an average diameter of 90 nm and a surface charge of +51 mV (Figure 5C), strongly interacted with the MCS. The *f*-QD-L localized 30–50-μm deep within the MCS mass, as shown by CLSM. Zwitterionic *f*-QD-L that contained DOPC:DOPE:-Chol (2:1:1.5) and a similar average diameter but a weak negative surface charge of −16 mV (Figure 5D) were able to diffuse deeper into the spheroids; therefore, a less intense fluorescence signals but more uniform distribution was observed within MCS.

2.5. Intratumoral Administration of *f*-QD-L Hybrid Nanoparticles In Vivo

In order to translate the findings obtained from the interaction of *f*-QD-L hybrids with the avascular in vitro tumor microenvironment model (MCS) to a vascularized, more complex in vivo solid tumor model, syngeneic solid tumor models were implanted subcutaneously and grown in C57Bl6

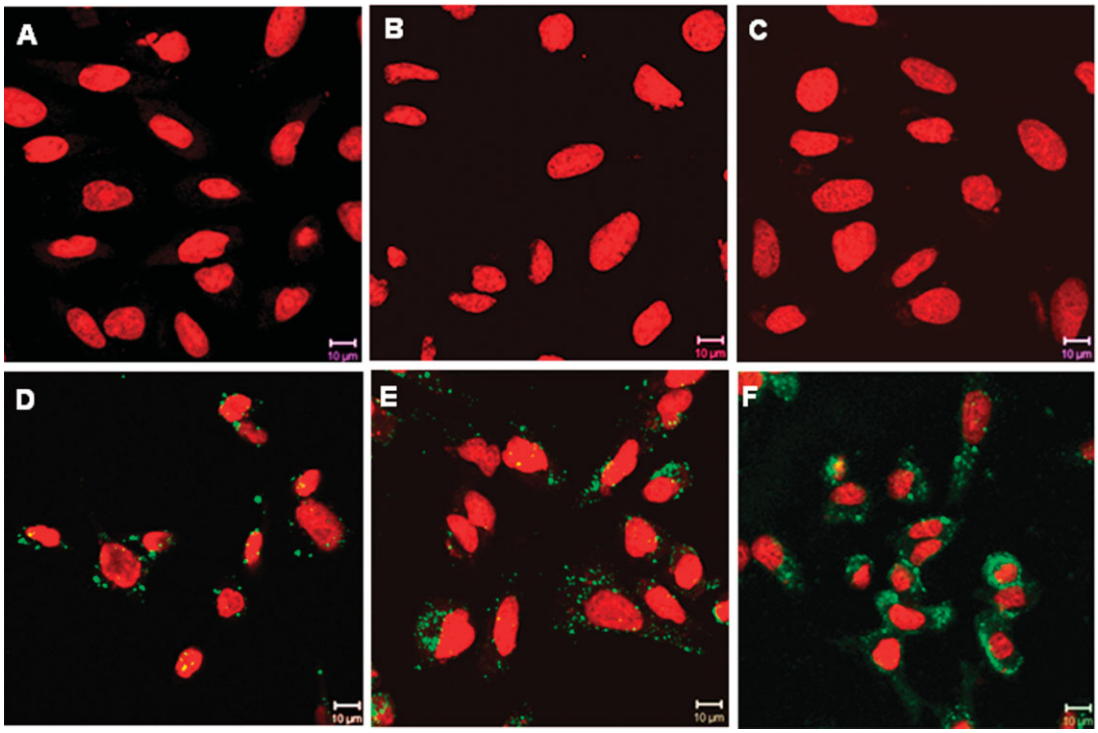

Figure 4. Tumor-cell internalization of *f*-QD-L hybrid nanoparticles. CLSM images of A549 monolayer after 3 h incubation with *f*-QD at A) 40 nM, B) 80 nM, C) 145 nM, and *f*-QD-L [DOPC:DC-Chol (10:1)] at D) 40 nM, E) 80 nM, and F) 145 nM. Cells were fixed with 4% PFA and nuclei were counterstained with PI. Scale bar is 10 μm in all images.

mice. *f*-QD, *f*-QD-L and fluorescently DiI-labeled SUV alone were injected intratumorally into a fully grown, B16F10 melanoma tumor model. The animals were injected with a dose of 33 pmol of *f*-QD alone or within zwitterionic or cationic *f*-QD-L and compared with control DiI-labeled liposomes alone. The animals were killed 5 min and 24 h after injection, tumors were snap frozen, cryosectioned, fixed, and imaged. The cell nuclei were counterstained with PI to evaluate the QD

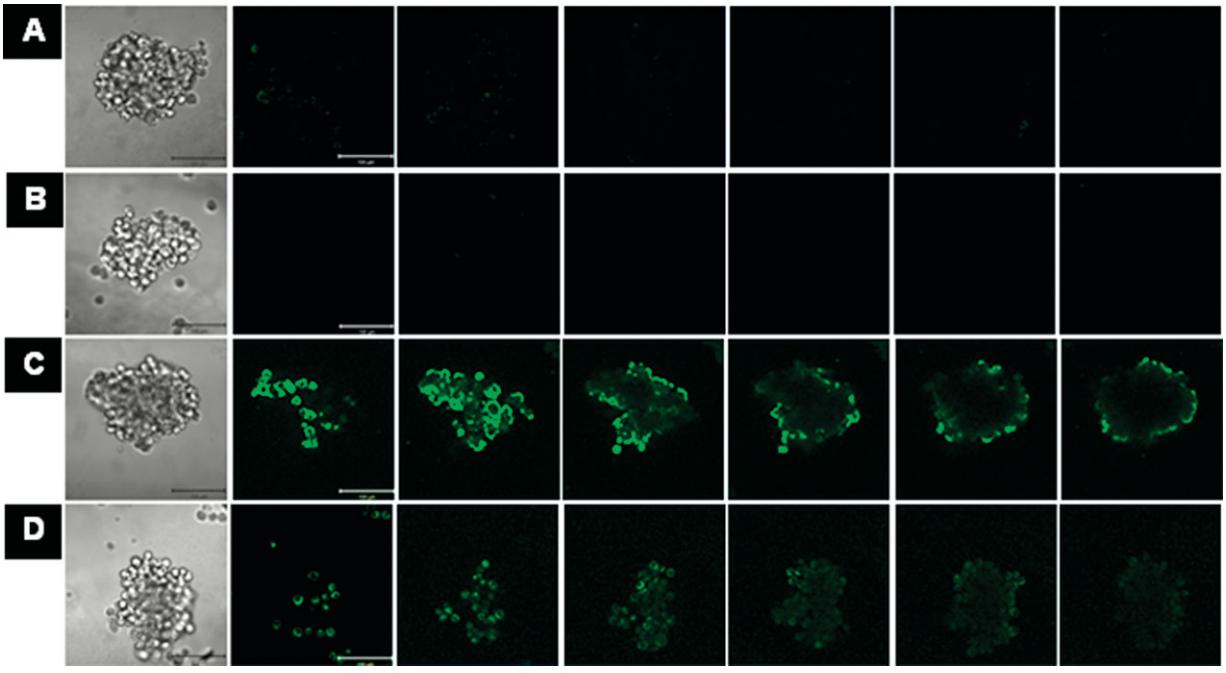

Figure 5. 3D multicellular tumor spheroid penetration of *f*-QD-L hybrid nanoparticles. Light and CLSM images of B16F10 multicellular spheroids (MCS) incubated for 4 h with A) serum-free DMEM and 145 nM *f*-QD, B) alone, C) in cationic *f*-QD-L [DOPC:DOPE:Chol:DC-Chol (2:1:1.5:0.3)], and D) in zwitterionic *f*-QD-L [DOPC:DOPE:Chol (2:1:1.5)]. Optical sections at 0, 16, 32, 48, 64, and 80-μm thickness from the top towards the tumor spheroid equatorial plane are shown (left to right). The images are representative of at least 30 spheroids imaged. Scale bar is 100 μm throughout.

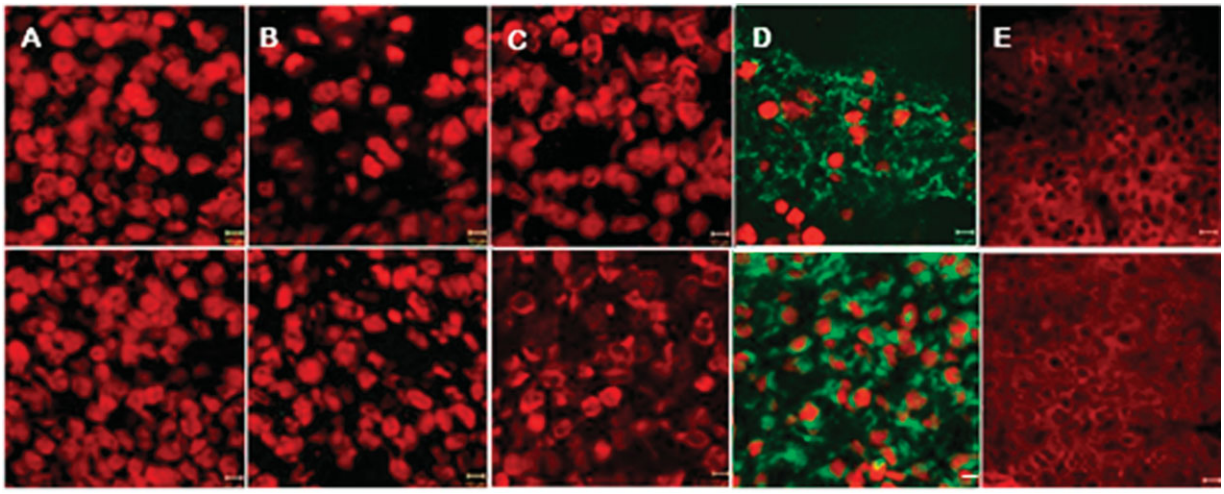

Figure 6. In vivo solid tumor model penetration and labeling by *f*-QD-L hybrid nanoparticles. CLSM images of B16F10 tumors dissected 5 min (top panel) and 24 h (lower panel) after intratumoral injection with A) 5% dextrose, 33 pmol B) *f*-QD alone, C) zwitterionic *f*-QD-L [DOPC:Chol], D) cationic *f*-QD-L [DOPC:DOPE:Chol:DC-Chol], and E) DiI-labeled SUV alone [DOPC:DOPE:Chol:DC-Chol]. Scale bar is 10 μm.

tumor localization, retention, and distribution within the tumor volume under the CLSM of the sectioned tissue.

Low fluorescence signals were detected in tumor sections injected with *f*-QD and zwitterionic *f*-QD-L (DOPC:Chol) hybrids as soon as 5 min post-injection (Figure 6B and C). In contrast, high-intensity green-fluorescence signals were obtained from the tumors injected with cationic *f*-QD-L (DOPC:DOPE:Chol:DC-Chol) after both 5 min and 24 h. After 5 min, the cationic *f*-QD-L were localized into the intercellular space of the tumor interstitium or bound to the tumor cell membranes (Figure 6D, upper panel). At 24 h post-administration, the *f*-QD-L were uptaken by tumor cells and close to the nucleus (Figure 6D, lower panel). Remarkable similarity was therefore found between the in vivo solid tumor model sections and the in vitro tumor cellular internalization of *f*-QD-L. Moreover, both empty DiI-labeled liposomes (Figure 6E) and *f*-QD-L hybrid nanoparticles consisting of the same lipid composition (Figure 6D) exhibited very similar intratumoral binding, retention, and distribution profiles.

3. Discussion

Quantum dots have been used as fluorescent tags of cells for in vitro and in vivo imaging of different cell types without affecting cell viability and function.[8,11,39] Many ex vivo techniques have been employed to achieve efficient QD cell labeling such as microinjection,[9,13] electroporation,[13,15] and lipid-mediated transfection.[10,13] Electroporation, even though effective, is not a convenient technique to label large numbers of cells and generally suffers from extensive cell death. Moreover, electroporation has also been found to induce QD aggregation (500 nm) on application of the electrical field.[13] Although microinjection has been shown to be superior to electroporation for individual cell labeling by QD, each cell needs to be manipulated separately.[9,13] Preformed cationic liposome complexes with nucleic acids, magnetic nanoparticles[40,41] as well as *f*-QD[4,5,10,13,14] can bind to the plasma membrane, mediate endocytosis, and have been shown to lead to intracellular delivery. Previous studies have only reported mixing of water-soluble *f*-QDs with preformed cationic liposomes to enhance plasma-membrane translocation. Derfus et al. and Hsieh et al. showed high labeling efficiency using *f*-QD complexed with Lipofectamine (a commercially available cationic lipid-based reagent) compared to other carriers.[13,14] More recently, our laboratory and others reported hydrophobic QD that self-assembled as part of the lipid bilayer of vesicles, suitable for cell labeling.[42–44] However, such QD vesicles are only feasible with QD that have average sizes smaller than the thickness of the lipid bilayer (approximately 4 nm), while larger QD do not lead to vesicle self-assembly.[43,44] Engineering *f*-QD-L hybrids described in the present study offers more flexibility since functionalized QD up to 50 nm in diameter can be used, with a wide variety of lipid combinations, such as pH-sensitive lipids or other endosome disruptive agents.

Several groups have functionalized QD surfaces with ligands that promote receptor-mediated endocytosis[11,45] and, more recently, intracellular translocation of QD via peptide-mediated delivery.[18,22,26,27,46] However, decorating the QD surface with certain ligands can quench QD fluorescence as previously described.[47] Moreover, very recent investigations by Clarke et al. [48] indicate that QD fluorescence intensity, surface charge, colloidal stability, and interaction with cells depend on the ligand density at the QD surface. This study also reported significant variations during ligand conjugation among QD of different sizes and surface characteristics.

PEGylated QD that are the most relevant to in vivo applications have been reported to exhibit minimum non-specific cellular binding.[5,12–14] Hsieh et al. reported no cell labeling when human bone marrow stem cells (hBMSC) were incubated with COOH-PEG-coated QD. Derfus et al. reported green-fluorescence aggregates of low intensity at the extracellular border once the cells were incubated with PEG-coated

QD. Generally, the need for a versatile approach to label cells efficiently in a modular fashion that can be adapted easily for both in vitro and in vivo applications has emerged as many different types of QD systems are being developed with potentially interesting biomedical applications.

In this work, we attempted to fulfill that need by describing a general methodology for the engineering of *f*-QD-L hybrid nanoparticles by incorporation of *f*-QD into lipid vesicles. These systems can be used to deliver intracellularly a wide range of QD regardless of the QD core size and without the need for conjugation chemistry on the QD surface. Moreover, *f*-QD-L hybrid systems were shown to interact, penetrate, localize and be retained by tumor cells in vivo.

Several studies have also reported QD targeting to tumors by intravenous administration.[6,8,17,19,21,25,49] Conjugations of specific antibodies onto the QD surface increased tumor targeting contrary to nonfunctionalized QD.[17,19,25,49] However, such strategies have not yet shown penetration of QD from the regions close to tumor vasculature deeper into the tumor mass.[6,17,49] Intratumoral (i.t.) administration offers an alternative in order to either label solid tumor cells (to monitor their migratory patterns) or deliver cytotoxic agents locally at the tumor site, and is clinically relevant for well-localized solid tumors (e.g., head and neck, cerebral carcinomas). However, rapid clearance by the lymphatic drainage system is still the main obstacle for widespread clinical use, as has been recently validated by injecting radiolabeled colloids into breast-cancer patients to map their sentinel lymph nodes.[50,51] Very recently, a study has reported direct injection of neutral (methoxy), negatively (carboxy), and positively (amine) charged PEG-coated QD into solid tumor xenografts, reporting their rapid clearance to the lymph nodes[30] and use of QD for lymph-node imaging. In fact, the most clinically developed studies are using QD as potential lymph-node contrast agent markers.[52–58] Frangioni and colleagues have studied extensively near-infrared (NIR) QD as imaging agents for sentinel lymph nodes (SLN) in small and large animals, and mapped SLN of the pleural space,[54] oesophagus,[55] and lung.[58] Interestingly, all such studies have successfully shown that 15–20-nm NIR QD were immediately uptaken by SLN after local injection. They were more selective for localization to the first draining lymph nodes and no migration to distant nodes was observed;[53,54] therefore, NIR QD were considered superior to vital blue dye and ^{99m}Tc colloids[54] as lymph-node contrast agents.

Localization and retention of different anticancer drugs and delivery systems in the tumor mass by i.t. administration has also been extensively studied.[59–62] The clearance rate from the tumor volume is highly dependent on the nanoparticle molecular weight and surface charge. Nomura et al. studied the correlation between the particle size and surface charge and the retention into tissue-isolated tumors after intratumoral injection.[60] They found zwitterionic delivery systems (emulsions and liposomes) around 100 nm in diameter were leaking from the tumor immediately after administration. On the other hand, positively charged particles with similar sizes significantly increased tumor retention.[62] Similar results were obtained following intratumoral administration of low-molecular-weight mitomycin C conjugated to cationic dextran.[62] In the case of *f*-QD, Ballou et al. reported indistinguishable drainage of 20–40 nm PEG QD with neutral, negative, and positive surface charges to the lymph nodes immediately after intratumoral administration.[30] Due to their small size PEG QD localized in the lymphatic tissue within 3–4 min after injection.[53] Such data is in direct agreement with our observations herein, whereby small, PEG-coated QD were shown not to be uptaken by tumor cells in monolayers (Figure 4), not interacting or penetrating tumor cell spheroids (Figure 5), and not retained or localized within solid tumor models in vivo (Figure 6). This is thought to be due to the steric hindrance of the lipopolymer coat at the QD surface, as has been previously described for PEGylated liposomes.[37] Overall, these results indicate that uncharged *f*-QD or *f*-QD-L hybrid nanoparticles do not interact with tumor cells in vitro and are drained rapidly from the tumor interstitium (presumably through the lymphatic drainage system) in vivo. In the present work we engineered cationic and fusogenic *f*-QD-L hybrid nanoparticles to electrostatically interact with the tumor cell membrane in vitro, localize, and be retained within the tumor interstitium and tumor cells in vivo.

4. Conclusions

The hybrid *f*-QD-L nanoparticles engineered in this study were shown to be efficiently uptaken by living cells in the absence of cell death and can therefore be used as fluorescent probes for ex vivo cell-labeling studies with most types of water-soluble QD without further modification. Most importantly though, *f*-QD-L exhibited enhanced penetration and retention into the tumor interstitium both in vitro (tumor spheroids) and in vivo (subcutaneous solid tumors). This hybrid system offers further opportunities as a platform for fabrication of combinatory therapeutic (if drug molecules can be encapsulated in the *f*-QD-L) and imaging (via the *f*-QD) modalities. Further work is also needed to evaluate the pharmacokinetic profile and systemic toxicity of such hybrid systems in vivo after local and systemic administration before any clinical development.

5. Experimental Section

Materials: Carboxyl-functionalized PEG-coated QD (COOH-PEG-QD), Evident Technologies (New York, USA). Dioleoylphosphatidylcholine (DOPC), Lipoid GmbH (Germany). DC-cholesterol and DOPE, Avanti Polar Lipid (USA). 1,1′, dioctadecyl-3, 3,3′, 3′-tetramethyl-indocarbocynine perchlorate (DiI); propidium iodide (PI), Molecular Probes (USA). Dulbecco's modified Eagle medium (DMEM); HAM F12; Advanced RPMI-1640; foetal bovine serum (FBS); penicillin/streptomycin; phosphate buffer saline (PBS), Invitrogen (UK). Cholesterol (Chol); RNAse A enzyme, Sigma (UK).

f-QD-L preparation: DOPC, DOPC:DC-Chol (10:1), DOPC:Chol (2:1), DOPC: DOPE:Chol (2:1:1.5), and DOPC:DOPE:Chol:DC-Chol (2:1:1.5:0.3) molar ratio were dissolved in chloroform: methanol (4:1 v/v). Multilamellar vesicles (MLV) were prepared by evaporating the organic solvent using a rotovaporator (BÜCHI, Switzerland)

NANO MICRO small

under vacuum for 30 min at 40 °C then flushed with N_2 stream to remove any residual traces of organic solvent. The dried lipid film was initially hydrated with (13.7 μL) of *f*-QD (stock concentration 12 μM) suspension, followed by addition of (200 μL) fractions of dH_2O up to a final volume of (1 mL). *f*-QD-L hybrids were prepared by bath sonication (Ultrasonic cleaner, VWR) for 10 min at 30 °C. Final lipid concentrations were 0.4, 4, 8, and 20 mM, corresponding to a final QD concentration of 1×10^{14} p mL^{-1} (160 nM). The *f*-QD-L mean average diameter and surface charge in dH_2O were measured by Zetasizer Nano ZS, Malvern (UK).

Agarose gel electrophoresis: 40 μL aliquot of freshly prepared COOH-PEG-QD, *f*-QD-L, and QD SUV mixture at different lipid concentrations of DOPC was mixed with 8 μL of 30% (w/v) glycerol in 0.5× TBE buffer, and loaded to 1% agarose gel (0.25× TBE) in 0.5× TBE buffer. The gel was run for 60 min at 80 V using a subcell GT agarose gel electrophoresis system (BioRad, USA) and then photographed under UV light using GeneGenius system, PerkinElmer Life, and Analytical Sciences (USA).

Cryo-TEM: Sample preparation for cryo-TEM was carried out in a temperature- and humidity-controlled chamber using a fully automated (pc-controlled) vitrification robot (Vitrobot, patent applied), as previously described.[63] The grids with vitrified thin films were analyzed in a CM-12 transmission microscope (Philips, Eindhoven, The Netherlands) at −170 °C using a Gatan-626 cryo-specimen holder and cryotransfer system (Gatan, Warrendale, PA).

Interaction of f-QD-L hybrid nanoparticles with mammalian cell cultures: Human-lung adenocarcinoma cell line A549 (ATCC, USA), was grown to confluency on glass coverslips in 24-well tissue culture dishes (Corning B.V., The Netherlands) at a density of 50 000 cells per well in F12 Ham media supplemented with 10% FBS and 1% penicillin/streptomycin. Cells were incubated with 0.5 mL of COOH-PEG-QD or *f*-QD-L of DOPC: DC-Chol (10:1), at 7.2 mM (145 nM QD), 3.8 mM (80 nM QD), and 1.8 mM (40 nM QD) lipid concentrations for 1 and 3 h. To remove unbound *f*-QD-L, cells were washed with warm PBS, fixed with 4% paraformaldehyde (PFA) in PBS for 15 min at room temperature, and rinsed with PBS. For nuclear staining, cells were permeabilised with 0.1% Triton X-100 in PBS for 10 min at room temperature, RNAase treated (100 μg mL^{-1}) for 20 min at 37 °C, and incubated with propidium iodide (1 μg mL^{-1}) in PBS for 1–5 min, then rinsed three times with PBS. Cover slips were mounted with aqueous poly(vinyl alcohol) Citiflour reagent mixed with AF100 antifade reagent (1:10) prior use (Citiflour, UK). Slides were studied with a confocal laser scanning microscope (Zeiss LSM 510 Meta). The lasers used were a 30 mW Argon laser (488 nm for green channel) and a 1 mW 543-nm HeNe laser (for red channel). The emission was collected using a band-pass filter between 505–530 nm for green QD and 560-nm long-pass filter for PI. Slides were visualized under 63× oil-immersion lens.

Spheroid penetration study: B16F10, a melanoma murine cancer-cell line, was grown to confluency in a T-75 tissue culture flask (Corning B.V., The Netherlands) in advanced RPMI-1640 supplemented with 10% FBS, 2 mM L-Glutamine and 1% penicillin/streptomycin. Multicellular spheroids (MCS) were prepared randomly according to the liquid overlay technique of Yuhas et al.,[64] approximately 2×10^6 cells, obtained by trypsinization from a growing monolayer culture, were seeded into 100-mm dishes coated with a thin layer of 1% agar (Bacto Agar; Difco, detroit, MI) with 15 mL of the complete media. After 3–5 days in the agar culture, spheroids 150–200 μm in diameter were observed under an inverted phase-contrast microscope with an ocular graticule. Spheroids were subsequently used for penetration experiments. Approximately, 200 spheroids were incubated with COOH-PEG-QD or *f*-QD-L, prepared as mentioned previously, at a final lipid concentration of 7.2 mM (145 nM QD) for 4 h. Spheroids were rinsed with warm PBS before transfer to a glass-bottom 24-well plate and viewed using CLSM using 40× oil-immersion lens.

Animals and tumor model: All animal experiments were performed in compliance with the UK Home Office Code of Practice for the Housing and Care of Animals used in Scientific Procedures. 10–12-week-old female C57bl6 mice (Harlan UK Limited, UK) were caged in groups of 5 with free access to water. A temperature of 19–22 °C was maintained with a relative humidity of 45–65%, and a 12 h light–dark cycle. Animals were acclimatized for 7 days before each experiment. Mice were inoculated subcutaneously with 1×10^6 B16F10 melanoma cells in a volume of 100 μL PBS into the shaved right flank using 26G needles. The tumor volume was estimated by measuring three orthogonal diameters (*a*, *b*, and *c*) with calipers; the volume was calculated as $(a \times b \times c) \times 0.5$ mm^3. Intratumoral injections were performed when the tumor reached 500 mm^3.

Intratumoral administration and tissue analysis: Mice were anaesthetized using isofluorane, and 50 μL of the COOH-PEG-QD, *f*-QD-L composed of DOPC: Chol (2:1), DOPC:DOPE: Chol:DC-Chol (2:1:1.5:0.3), prepared as described earlier, or DiI-labelled DOPC: DOPE: Chol: DC-Chol (2:1:1.5:0.3) prepared as described elsewhere[37] and used here as a positive control. The needle was inserted into the longitudinal direction from the tumor edge into the centre of the tumor and 50 μL was administered slowly over 1 min and the needle was left in the tumor for another 5 min to prevent sample leakage. 5 min and 24 h later, the mice were killed and tumor tissue was harvested and snap-frozen immediately into liquid-nitrogen-cooled isopentane. Samples were stored at −80 °C prior to frozen sectioning. Frozen tumors were embedded into OCT and plunged into a liquid-nitrogen bath for at least 30 s. Samples were retrieved from the bath then sectioned using the cryostat at −18 °C into 5–6-μm-thick sections. The sections were mounted on a superfrost slide and left to dry at room temperature for 15–30 min. For tumor visualization, the sections were fixed for 3 min in cold acetone at −20 °C, rinsed with PBS for 15 min at room temperature, followed by PI nuclear staining as described previously and visualized under 63× oil immersion lens using CLSM.

Acknowledgements

This work was partially supported by The School of Pharmacy, University of London. The authors acknowledge Lipoid Co. (Germany) for the lipid samples and Evident Technologies (New York, USA) for the collaborative agreement on the provision of quantum dots, Ms. Jennifer Podesta for her help with gel electrophoresis, Mr. Ravi Singh for his advice in the

animal work, and Mr. Stephen Davison (The Department of Histopathology and Cytopathology, Royal Free Hospital) for tumor cryosectioning. W.A.-J. is a recipient of the Overseas Research Student Award Scheme (ORSAS) from the University of London. K.A.-J. is a recipient of the Maplethorpe Fellowship, The University of London.

[1] W. J. Parak, R. Boudreau, M. Le Gros, D. Gerion, D. Zanchet, C. M. Micheel, S. C. Williams, A. P. Alivisatos, C. Larabell, *Adv. Mater.* **2002**, *14*, 882.
[2] R. Tombolini, J. K. Jansson, *Methods Mol. Biol.* **1998**, *102*, 285.
[3] X. Gao, L. Yang, J. A. Petros, F. F. Marshall, J. W. Simons, S. Nie, *Curr. Opin. Biotechnol.* **2005**, *16*, 63.
[4] A. A. Chen, A. M. Derfus, S. R. Khetani, S. N. Bhatia, *Nucleic Acids Res.* **2005**, *33*, 190.
[5] C. Srinivasan, J. Lee, F. Papadimitrakopoulos, L. K. Silbart, M. Zhao, D. J. Burgess, *Mol. Ther.* **2006**, *14*, 192.
[6] M. E. Akerman, W. C. Chan, P. Laakkonen, S. N. Bhatia, E. Ruoslahti, *Proc. Natl. Acad. Sci. U. S. A* **2002**, *99*, 12617.
[7] A. P. Alivisatos, *Science* **1996**, *271*, 933.
[8] X. Michalet, F. F. Pinaud, L. A. Bentolila, J. M. Tsay, S. Doose, J. J. Li, G. Sundaresan, A. M. Wu, S. S. Gambhir, S. Weiss, *Science* **2005**, *307*, 538.
[9] B. Dubertret, P. Skourides, D. J. Norris, V. Noireaux, A. H. Brivanlou, A. Libchaber, *Science* **2002**, *298*, 1759.
[10] E. B. Voura, J. K. Jaiswal, H. Mattoussi, S. M. Simon, *Nat. Med.* **2004**, *10*, 993.
[11] J. K. Jaiswal, H. Mattoussi, J. M. Mauro, S. M. Simon, *Nat. Biotechnol.* **2003**, *21*, 47.
[12] W. J. Parak, T. Pellegrino, C. Plank, *Nanotechnology* **2005**, *16*, R9–R25.
[13] A. M. Derfus, W. C. Chan, S. N. Bhatia, *Adv. Mater.* **2004**, *16*, 961.
[14] S. C. Hsieh, F. F. Wang, C. S. Lin, Y. J. Chen, S. C. Hung, Y. J. Wang, *Biomaterials* **2006**, *27*, 1656.
[15] F. Q. Chen, D. Gerion, *Nano Lett.* **2004**, *4*, 1827.
[16] V. Bagalkot, L. Zhang, E. Levy-Nissenbaum, S. Jon, P. W. Kantoff, R. Langer, O. C. Farokhzad, *Nano Lett.* **2007**, *7*, 3065.
[17] W. Cai, D. W. Shin, K. Chen, O. Gheysens, Q. Cao, S. X. Wang, S. S. Gambhir, X. Chen, *Nano Lett.* **2006**, *6*, 669.
[18] J. B. Delehanty, I. L. Medintz, T. Pons, F. M. Brunel, P. E. Dawson, H. Mattoussi, *Bioconjug. Chem.* **2006**, *17*, 920.
[19] P. Diagaradjane, J. M. Orenstein-Cardona, E. Colon-Casasnovas, A. Deorukhkar, S. Shentu, N. Kuno, D. L. Schwartz, J. G. Gelovani, S. Krishnan, *Clin. Cancer Res.* **2008**, *14*, 731.
[20] A. Jayagopal, P. K. Russ, F. R. Haselton, *Bioconjug. Chem.* **2007**, *18*, 1424.
[21] H. Tada, H. Higuchi, T. M. Wanatabe, N. Ohuchi, *Cancer Res.* **2007**, *67*, 1138.
[22] Y. Zhang, M. K. So, J. Rao, *Nano Lett.* **2006**, *6*, 1988.
[23] H. Duan, S. Nie, *J. Am. Chem. Soc.* **2007**, *129*, 3333.
[24] W. Liu, M. Howarth, A. B. Greytak, Y. Zheng, D. G. Nocera, A. Y. Ting, M. G. Bawendi, *J. Am. Chem. Soc.* **2008**, *130*, 1274.
[25] X. Gao, Y. Cui, R. M. Levenson, L. W. Chung, S. Nie, *Nat. Biotechnol.* **2004**, *22*, 969.
[26] B. C. Lagerholm, M. M. Wang, L. A. Ernst, D. H. Ly, H. J. Liu, M. P. Bruchez, A. S. Waggoner, *Nano Lett.* **2004**, *4*, 2019.
[27] S. M. Rozenzhak, M. P. Kadakia, T. M. Caserta, T. R. Westbrook, M. O. Stone, R. R. Naik, *Chem. Commun.* **2005**, 2217.
[28] G. Ruan, A. Agrawal, A. I. Marcus, S. Nie, *J. Am. Chem. Soc.* **2007**, *129*, 14759.
[29] K. Susumu, H. T. Uyeda, I. L. Medintz, T. Pons, J. B. Delehanty, H. Mattoussi, *J. Am. Chem. Soc.* **2007**, *129*, 13987.
[30] B. Ballou, L. A. Ernst, S. Andreko, T. Harper, J. A. Fitzpatrick, A. S. Waggoner, M. P. Bruchez, *Bioconjug. Chem.* **2007**, *18*, 389.
[31] D. D. Lasic, D. Papahadjopoulos, *Medical Applications of Liposomes*, Elsevier Science, Amsterdam, **1998**.
[32] S. K. Dixit, N. L. Goicochea, M. C. Daniel, A. Murali, L. Bronstein, M. De, B. Stein, V. M. Rotello, C. C. Kao, B. Dragnea, *Nano Lett.* **2006**, *6*, 1993.
[33] T. Pons, H. T. Uyeda, I. L. Medintz, H. Mattoussi, *J. Phys. Chem. B. Condens. Matter Mater. Surf. Interfaces. Biophys.* **2006**, *110*, 20308.
[34] D. R. Larson, W. R. Zipfel, R. M. Williams, S. W. Clark, M. P. Bruchez, F. W. Wise, W. W. Webb, *Science* **2003**, *300*, 1434.
[35] A. Wolcott, D. Gerion, M. Visconte, J. Sun, A. Schwartzberg, S. Chen, J. Z. Zhang, *J. Phys. Chem. B. Condens. Matter Mater. Surf. Interfaces. Biophys.* **2006**, *110*, 5779.
[36] K. A. Walker, R. Mairs, T. Murray, T. E. Hilditch, T. E. Wheldon, A. Gregor, I. M. Hann, *Cancer Res.* **1990**, *50*, 1000s.
[37] K. Kostarelos, D. Emfietzoglou, A. Papakostas, W. H. Yang, A. Ballangrud, G. Sgouros, *Int. J. Cancer* **2004**, *112*, 713.
[38] G. Gregoriadis, C. Davis, *Biochem. Biophys. Res. Commun.* **1979**, *89*, 1287.
[39] M. Stroh, J. P. Zimmer, D. G. Duda, T. S. Levchenko, K. S. Cohen, E. B. Brown, D. T. Scadden, V. P. Torchilin, M. G. Bawendi, D. Fukumura, R. K. Jain, *Nat. Med.* **2005**, *11*, 678.
[40] K. Hirao, T. Sugita, T. Kubo, K. Igarashi, K. Tanimoto, T. Murakami, Y. Yasunaga, M. Ochi, *Int. J. Oncol.* **2003**, *22*, 1065.
[41] M. Shinkai, M. Yanase, H. Honda, T. Wakabayashi, J. Yoshida, T. Kobayashi, *Jpn. J. Cancer Res.* **1996**, *87*, 1179.
[42] L. Feng, X. Kong, K. Chao, Y. Sun, Q. Zeng, Y. Zhang, *Mater. Chem. Phys.* **2005**, *93*, 310.
[43] G. Gopalakrishnan, C. Danelon, P. Izewska, M. Prummer, P. Y. Bolinger, I. Geissbuhler, D. Demurtas, J. Dubochet, H. Vogel, *Angew. Chem.* **2006**, *118*, 5604. *Angew. Chem. Int. Ed* **2006**, *45*, 5478.
[44] W. T. Al-Jamal, K. T. Al-Jamal, B. Tian, L. Lacerda, P. H. Bomans, P. M. Frederik, K. Kostarelos, *ACS Nano* **2008**, *2*, 408.
[45] W. J. Mulder, R. Koole, R. J. Brandwijk, G. Storm, P. T. Chin, G. J. Strijkers, C. de Mello Donega, K. Nicolay, A. W. Griffioen, *Nano Lett.* **2006**, *6*, 1.
[46] J. Silver, W. Ou, *Nano Lett.* **2005**, *5*, 1445.
[47] S. J. Clarke, C. A. Hollmann, Z. Zhang, D. Suffern, S. E. Bradforth, N. M. Dimitrijevic, W. G. Minarik, J. L. Nadeau, *Nat. Mater.* **2006**, *5*, 409.
[48] S. J. Clarke, C. A. Hollmann, F. A. Aldaye, J. L. Nadeau, *Bioconjug. Chem.* **2008**.
[49] W. Cai, K. Chen, Z. B. Li, S. S. Gambhir, X. Chen, *J. Nucl. Med.* **2007**, *48*, 1862.
[50] D. Krag, D. Weaver, T. Ashikaga, F. Moffat, V. S. Klimberg, C. Shriver, S. Feldman, R. Kusminsky, M. Gadd, J. Kuhn, S. Harlow, P. Beitsch, *N. Engl. J. Med.* **1998**, *339*, 941.
[51] I. T. Rubio, S. Korourian, C. Cowan, D. N. Krag, M. Colvert, V. S. Klimberg, *Am. J. Surg.* **1998**, *176*, 532.
[52] Y. Hama, Y. Koyama, Y. Urano, P. L. Choyke, H. Kobayashi, *Breast Cancer Res. Treat.* **2006**.
[53] S. Kim, Y. T. Lim, E. G. Soltesz, A. M. De Grand, J. Lee, A. Nakayama, J. A. Parker, T. Mihaljevic, R. G. Laurence, D. M. Dor, L. H. Cohn, M. G. Bawendi, J. V. Frangioni, *Nat. Biotechnol.* **2004**, *22*, 93.
[54] C. P. Parungo, Y. L. Colson, S. W. Kim, S. Kim, L. H. Cohn, M. G. Bawendi, J. V. Frangioni, *Chest* **2005**, *127*, 1799.
[55] C. P. Parungo, S. Ohnishi, S. W. Kim, S. Kim, R. G. Laurence, E. G. Soltesz, F. Y. Chen, Y. L. Colson, L. H. Cohn, M. G. Bawendi, J. V. Frangioni, *J. Thorac. Cardiovasc. Surg.* **2005**, *129*, 844.
[56] E. G. Soltesz, S. Kim, S. W. Kim, R. G. Laurence, A. M. De Grand, C. P. Parungo, L. H. Cohn, M. G. Bawendi, J. V. Frangioni, *Ann. Surg. Oncol.* **2006**, *13*, 386.

[57] J. P. Zimmer, S. W. Kim, S. Ohnishi, E. Tanaka, J. V. Frangioni, M. G. Bawendi, *J. Am. Chem. Soc.* **2006**, *128*, 2526.
[58] E. G. Soltesz, S. Kim, R. G. Laurence, A. M. DeGrand, C. P. Parungo, D. M. Dor, L. H. Cohn, M. G. Bawendi, J. V. Frangioni, T. Mihaljevic, *Ann. Thorac. Surg.* **2005**, *79*, 269.
[59] K. J. Harrington, G. Rowlinson-Busza, K. N. Syrigos, P. S. Uster, R. G. Vile, J. S. Stewart, *Clin. Cancer Res.* **2000**, *6*, 2528.
[60] T. Nomura, N. Koreeda, F. Yamashita, Y. Takakura, M. Hashida, *Pharm. Res.* **1998**, *15*, 128.
[61] A. Bao, W. T. Phillips, B. Goins, X. Zheng, S. Sabour, M. Natarajan, F. Ross Woolley, C. Zavaleta, R. A. Otto, *Int. J. Pharm.* **2006**, *316*, 162.
[62] T. Nomura, A. Saikawa, S. Morita, T. Sakaeda Kakutani, F. Yamashita, K. Honda, Y. Takakura, M. Hashida, *J. Control Release* **1998**, *52*, 239.
[63] A. Moschetta, P. M. Frederik, P. Portincasa, G. P. vanBerge-Henegouwen, K. J. van Erpecum, *J. Lipid Res.* **2002**, *43*, 1046.
[64] J. M. Yuhas, A. P. Li, A. O. Martinez, A. J. Ladman, *Cancer Res.* **1977**, *37*, 3639.

Received: October 28, 2007
Revised: March 16, 2008

